Numerical evaluation of the behaviour of steel- and FRP-confined concrete columns using compression field modelling

E. Montoya [*], F.J. Vecchio, S.A. Sheikh

Department of Civil Engineering, University of Toronto, 35 St. George Street, Toronto, Canada M5S 1A4

Abstract

New constitutive models for confined concrete were formulated and implemented into in-house nonlinear finite element programs at the University of Toronto. A program for analysis of axisymmetric solids was specifically developed for this work. The confinement models proposed follow a compression field modelling approach that combines nonlinear elasticity and plasticity-type modelling. In this paper, the formulations are corroborated by examining the behaviour of reinforced concrete columns confined with fibre reinforced polymers (FRP), steel, or a combination of both. The analytical responses agree well with the experimental results, showing the capabilities of the models to reasonably model pre- and post-peak behaviour, and strength enhancement.

© 2004 Elsevier Ltd. All rights reserved.

Keywords: Confined concrete; Nonlinear analysis; Compression field modelling; Finite elements

1. Introduction

Compression field modelling of the behaviour of reinforced concrete was initially developed and verified for concrete in cracked states [1,2]; modelling of confined concrete was subsequently initiated with the work of Selby and Vecchio [3], who proposed preliminary three-dimensional formulations for confined concrete. These models were implemented in a nonlinear analysis program for reinforced concrete solids developed by Selby [4]. Some difficulties were encountered in trying to differentiate the load paths between the concrete cover and concrete core, and in the analytical post-peak behaviour of reinforced concrete columns subjected to monotonic axial compression. These difficulties were overcome in a study by Montoya et al. [5], where utilizing a set of well-known constitutive models and the compression field modelling approach, the characteristics of confined behaviour of reinforced concrete columns were better modelled. However, the preliminary confinement models implemented in the

analysis program did not cover all types of available concretes nor a wide range of confinement ratios (i.e. ratio of lateral pressure f_{cl} in concrete to unconfined concrete strength f_c').

In this paper, newly developed constitutive models for confined concrete were implemented in the nonlinear finite element analysis (NLFEA) programs VecTor3 and VecTor6 developed at the University of Toronto. The former is a general three-dimensional program for reinforced concrete solids, and the latter is a program for reinforced concrete solids of revolution developed for this work to analyze circular columns. The constitutive models include a stress–strain curve that accounts for three-dimensional effects, concrete dilatation, strength enhancement, post-peak softening or increased strain hardening. Concretes from low strength (20 MPa) to very high strength (120 MPa) subjected to confining pressure ratios from 0 to 100% of the concrete strength f_c', were studied. Compression field modelling utilizes a nonlinear elastic methodology whereby phenomenological and plasticity-type material models are combined and iterated until secant stiffness convergence is achieved at each load increment. This modelling approach does not require calibration of any

* Corresponding author. Tel./fax: +1-416-429-4074.
E-mail address: esneyder.montoya@utoronto.ca (E. Montoya).

parameter, as is the case with other types of modelling (e.g. [6,7]), or redetermination of parameters as a function of the type of loading (e.g. [8]).

2. Research significance

A set of stress–strain based constitutive models for triaxially compressed concrete contributes to the effectiveness of finite element techniques in providing insight into material and structural behaviour of reinforced concrete in a wide range of applications. Improved numerical modelling will assist in the study of rehabilitation and retrofitting of structural elements, and in the calibration of design formulae.

3. Compression field modelling of confined concrete

The set of constitutive material models used in the analysis of confined concrete is presented. Compression field modelling makes use of formulations derived from the modified compression field theory [2], and newly proposed models for confinement. A brief description of the models is given below; detailed background on the formulations is given elsewhere [9].

3.1. Concrete dilatation

The secant Poisson's ratio v_{ij}, that relates the strain in the direction j to the strain in the direction i, is proposed as a function of the compressive strain in the principal direction ε_{ci}, the strain at peak stress ε_{pi} in the direction i, and the average lateral pressure ratio normal to the plane j, f_{clj}/f_c'.

$$v_{ij} = v_0 + \left(1.9 + 24.2\frac{f_{clj}}{f_c'}\right)\frac{\varepsilon_{ci}}{\varepsilon_{pi}^2} \tag{1}$$

where v_0 is the initial Poisson's ratio. The average lateral pressure f_{clj} is calculated from:

$$f_{clj} = \frac{f_{ci} + f_{ck}}{2} \tag{2}$$

where f_{ci}, $f_{ck} < 0$, i and k are the principal directions normal to j. If $f_{ci} > 0$ or $f_{ck} > 0$, the lateral pressure is calculated as $f_{clj} = -f_{ck}$, $-f_{ci}$, respectively.

Experimental results of concrete cylinders subjected to triaxial compressive stresses, obtained from a testing program carried out by Imran and Pantazopoulou [10], were used to formulate the model.

3.2. Concrete in compression

Concrete in compression is modelled using two curves. For the pre-peak response, the model by Hoshikuma

et al. [11] was adopted:

$$f_{ci} = E_c\varepsilon_{ci}\left[1 + \frac{1}{n}\left(\frac{\varepsilon_{ci}}{\varepsilon_{pi}}\right)^{n-1}\right] \quad n = \frac{E_{ci}\cdot\varepsilon_{pi}}{E_{ci}\cdot\varepsilon_{pi} - f_{pi}} \tag{3}$$

where $i = 1, 2, 3$, denotes the principal stress directions, ε_{pi} and f_{pi} are the strain at peak and the peak stress, respectively. For post-peak behaviour, the following formulation is proposed, which is based on a modification of the analytical expression "the witch of Agnesi" (see [9]):

$$f_{ci} = \frac{f_{pi}}{A(\varepsilon_{ci}/f_{pi})^2 - B(\varepsilon_{ci}/f_{pi}) + C + 1.0} \tag{4}$$

where

$$A = k_d \quad B = 2\frac{A}{E_{sec}} \quad C = \frac{A}{E_{sec}^2}$$

$$E_{sec} = \frac{f_{pi}}{\varepsilon_{pi}} \quad k_d = \frac{1}{4}\left(\frac{f_{pi}}{\varepsilon_{c80i} - \varepsilon_{pi}}\right)^2 \tag{5}$$

The "shape" factor k_d is a function of the steepness of the post-peak behaviour of confined concrete, ε_{c80i} is the post-peak strain at 80% of the peak stress:

$$\frac{\varepsilon_{c80i}}{\varepsilon_{co}} = 1.5 + \left(89.5 - 0.60f_c'\right)\frac{f_{cl}}{f_c'} \tag{6}$$

A schematic representation of the stress–strain curve for concrete in compression is shown in Fig. 1, where the normalized stress, f_{pi}/f_c', increases with an increase in the confining pressure.

3.3. Concrete in tension

The average tensile stress–strain curve comprises an ascending linear elastic portion up to the tensile strength f_{ct}, and a descending portion that accounts for tension stiffening. The tensile strength of concrete f_{ct}
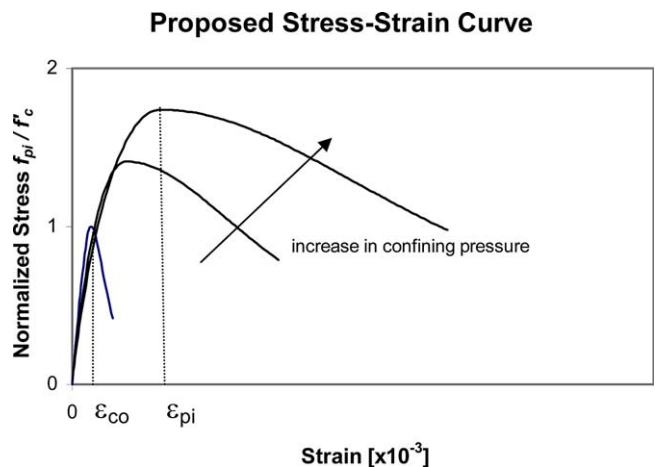

Proposed Stress-Strain Curve

Fig. 1. Schematic of the stress–strain curve for concrete in compression.

and the cracking strain ε_{cr} are obtained from the equations by Yamamoto and Vecchio [12]:

$$f_{ct} = 0.65 f_c'^{0.33} \qquad \varepsilon_{cr} = \frac{f_{ci}}{E_c} \qquad (7)$$

which were characteristic of high strength concrete tested at the University of Toronto. The ascending curve is given by

$$f_{ci} = E_c \varepsilon_{ci}, \qquad \varepsilon_{ci} < \varepsilon_{cr} \qquad (8)$$

and the descending curve is the tension stiffening model of Collins and Mitchell [1]

$$f_{ci} = \frac{f_{ci}}{1 + \sqrt{500 \varepsilon_{ci}}}, \qquad \varepsilon_{ci} > \varepsilon_{cr} \qquad (9)$$

3.4. Compression softening

The reduction of concrete strength due to crack opening in the principal tensile direction perpendicular to the major compression stress is calculated using the reduction factor β proposed by Vecchio [13]:

$$\beta = \frac{1}{1 + 0.55[0.35(-\varepsilon_{c1}/\varepsilon_{c3}) - 0.280]^{0.80}} \geq 1.0 \qquad (10)$$

3.5. Strength enhancement

The maximum stress f_{cc}, is calculated from the four-parameter Ottosen-type model:

$$a\frac{J_2}{f_c'^2} + \lambda\frac{\sqrt{J_2}}{f_c'} + b\frac{I_1}{f_c'} - 1 = 0$$
$$\lambda = k_1 + k_2 \cdot \cos 3\theta \qquad (11)$$

where the parameters are a, b, k_1, k_2, and the stress invariants I_1, J_2, and $\cos 3\theta$, are calculated as function of the principal stresses. Values for the parameter a are given in Table 1 as a function of the tensile strength f_{ct}. The remaining parameters are calculated as:

$$b = \frac{1}{9}a\left[\frac{f_{bc} - f_{ct}}{f_c'}\right] + \frac{1}{3}\left[\frac{f_c'}{f_{ct}} - \frac{f_c'}{f_{bc}}\right] \qquad (12)$$

$$k_1 = \frac{\sqrt{3}}{2}\left\{1 + \frac{f_c'}{f_{ct}} - \frac{1}{3}a\left[1 + \frac{f_{ct}}{f_c'}\right]\right\} \qquad (13)$$

$$k_2 = \frac{\sqrt{3}}{2}\left\{\frac{f_c'}{f_{ct}} - 1 - 2b - \frac{1}{3}a\left[\frac{f_{ct}}{f_c'} - 1\right]\right\} \qquad (14)$$

where the biaxial strength f_{bc} is obtained from Kupfer et al. [14].

$$f_{bc} = 1.16 f_c' \qquad (15)$$

The strength enhancement factor k_σ, due to confinement, can be written as:

$$k_\sigma = \frac{f_{cc}}{f_c'} \qquad (16)$$

The peak stress affected by strength enhancement and softening is calculated as:

$$f_{pi} = k_\sigma \cdot \beta \cdot f_c' \qquad (17)$$

3.6. Strain at peak stress

The proposed formulation for the strain at peak stress ε_{pi} is given by

$$\varepsilon_{pi} = k_s \cdot \beta \cdot \varepsilon_{co} \qquad (18)$$

where

$$k_s = 1.0 + \left(24.4 - 0.116 f_c'\right)\frac{f_{cl}}{f_c'} \qquad (19)$$

3.7. Cracking criterion

The Mohr–Coulomb criterion is used to determine the cracking stress f_{crf}, in triaxial states of stress

$$f_{crf} = \frac{2c \cdot \cos\phi}{1 + \sin\phi} \qquad c = f_c'\frac{1 - \sin\phi}{2\cos\phi} \qquad 0.20 \leq f_{cr}$$
$$= f_{crf}\left[1 + \frac{f_{c3}'}{f_c'}\right] \leq f_{ct} \qquad (20)$$

where c is the cohesion and $\phi = 37°$ is the angle of internal friction in concrete.

3.8. Steel and FRP composites

A bilinear curve with strain hardening is used to model steel in compression and tension. Bar buckling is not considered, and steel (or FRP) and concrete are assumed perfectly bonded. FRP fabrics are modelled using a linear elastic stress–strain curve that fails just after reaching the rupture stress.

4. Finite element analysis

The nonlinear elastic analysis procedure in VecTor3 and VecTor6 follow the nonlinear elastic methodology summarized below (see [4] for further details). The material stiffness matrix for each finite element is the

Table 1
Proposed values for parameter a

f_{ct} (MPa)	LN	HN	LH	HH
$0.65 f_c'^{0.33}$	17.097	2.406	17.447	15.061
$0.33 f_c'^{0.5}$	18.717	2.942	10.615	13.913
$0.60 f_c'^{0.5}$	8.070	1.103	4.633	6.668
$0.10 f_c'$	8.143	1.586	1.976	3.573

Notes: First letter L: low confinement ratio (≤ 0.20), H: high confinement ratio (> 0.20); Second letter N: normal strength concrete (≤ 40 MPa), H: high strength concrete (> 40 MPa).

sum of concrete and steel material matrices in global directions, $\mathbf{D}_c$ and $\mathbf{D}_s^i$, respectively, where i is the direction of each steel (or FRP) component.

$$\mathbf{D} = \mathbf{D}_c + \sum_n \mathbf{D}_s^i \tag{21}$$

$$\mathbf{D}_c = \mathbf{T}_c^T \mathbf{D}_c' \mathbf{T}_c \tag{22}$$

$$\mathbf{D}_s^i = \mathbf{T}_s^T \mathbf{D}_s'^i \mathbf{T} \tag{23}$$

where $\mathbf{D}_c'$ and $\mathbf{D}_s'^i$ are the material matrices in the principal directions, and $\mathbf{T}_c$ and $\mathbf{T}_s$ are the transformation matrices for concrete and steel, respectively. Dilatation strains are calculated using concept of prestrains [13]. The concrete dilatation vector $\boldsymbol{\varepsilon}_{co}'^T$ in the principal direction is given by

$$\boldsymbol{\varepsilon}_{co}'^T = \left\{ \begin{array}{ccc} \varepsilon_{co}^1 & \varepsilon_{co}^2 & \varepsilon_{co}^3 \end{array} \right\} \tag{24}$$

where

$$\varepsilon_{co}^i = -v_{ij}\frac{f_{cj}}{E_{cj}} - v_{ik}\frac{f_{ck}}{E_{ck}}, \quad i,j,k \text{ are principal directions} \tag{25}$$

The transformed concrete dilatations in the global direction are given by

$$\boldsymbol{\varepsilon}_{co} = \mathbf{T}_c \boldsymbol{\varepsilon}_{co}' \tag{26}$$

As concrete dilatation varies throughout the loading process, the prestrains due to dilation are converted to equivalent forces $\mathbf{F}_{co}$, applied to the finite element at each iteration.

$$\mathbf{F}_{co} = \mathbf{k}_c \boldsymbol{\delta}_{co} \tag{27}$$

where $\mathbf{k}_c$ is the concrete portion of the element stiffness matrix, and $\boldsymbol{\delta}_{co}$ is the equivalent displacement vector:

$$\boldsymbol{\delta}_{co} = \int_V \boldsymbol{\varepsilon}_{co} \, dV \tag{28}$$

These nodal forces are added to the externally applied forces on the structural element at each load step. The secant stiffness E_{ci} for the component materials is obtained from the stress–strain curves:

$$E_{ci} = \frac{f_{ci}}{\varepsilon_{ci}} \tag{29}$$

The flow chart in Fig. 2 shows this iterative analytical procedure. Program VecTor6 developed for this work, has a library of three axisymmetric elements: a four-node torus, a three-node torus, and a "ring" bar used to model steel spiral, hoops, and FRP layers. VecTor6 capabilities are limited to axisymmetric load. A detailed description of VecTor3 is given elsewhere [4].

5. Confined behaviour of reinforced concrete columns

Circular reinforced concrete columns confined with steel spirals, or steel spirals and fibre reinforced poly-mers (FRP), and square columns confined with different arrangements of lateral and longitudinal steel, subjected to monotonic axial loading, were examined using the compression field modelling approach described above. Stress–strain and axial load–axial strain curves obtained from experiments conducted by several researchers are compared to the finite element response. A brief description for each set of specimens is given along with the plots. In all cases, the values for the parameter a corresponding to a tensile strength $f_{ct} = 0.65f_c'^{0.33}$ were assumed in the analyses.

5.1. Demers and Neale columns [15]

The circular columns tested by these researchers were 300 mm in diameter and 1200 mm in length. All columns contained five bars of longitudinal steel. The researchers modelled corrosion by reducing by about 5 mm the diameter of the "noncorroded" bars in columns with the same properties. Stirrup spacing was either 150 or 300 mm, and the number of CFRP layers was kept constant in all the columns (three layers). Four of the 25 MPa columns tested were analyzed using program VecTor6. The properties for these columns are given in Table 2, where E_j is the stiffness of the CFRP, ε_{ju} is the ultimate strain of the CFRP, f_y and E_s are the yield strength and stiffness of the steel (assumed), respectively, d_b and d_t are the diameters of the longitudinal and lateral steel, respectively, and s is the spiral spacing. Due to symmetry only one quarter of each column was modelled using a mesh of 400 four-node torus. Imposed displacements were applied at the top of the column, and roller-type supports were added at the bottom of the mesh to allow for lateral displacement perpendicular to the loading. CFRP layers were modelled as ring bars with an area equal to the tributary area between adjacent nodes. The longitudinal steel was smeared in the axisymmetric elements. A sketch of the mesh is given Fig. 3 (left) for columns U25-2 and U25-3. The stirrup spacing was modified to 300 mm for columns U25-1 and U25-4, maintaining the same mesh.

Compression field modelling of these set of columns was carried out using a concrete strength of $0.85f_c'$, to account for size dependency of the plain concrete strength of the column. For brevity, the axial stress–axial strain curves for two of these columns are presented in Fig. 4, along with the analytical curves obtained with VecTor6 (solid thick lines). A compilation of the results is given in Table 3. The analytical model shows increasing stress with axial strain until failure (rupture of the fabric) for all the four columns, coinciding with the specimen failures. The peak strain coincides with the ultimate axial strain ε_{cfu} in all the analytical curves. The strain ε_{fu} is the measured strain
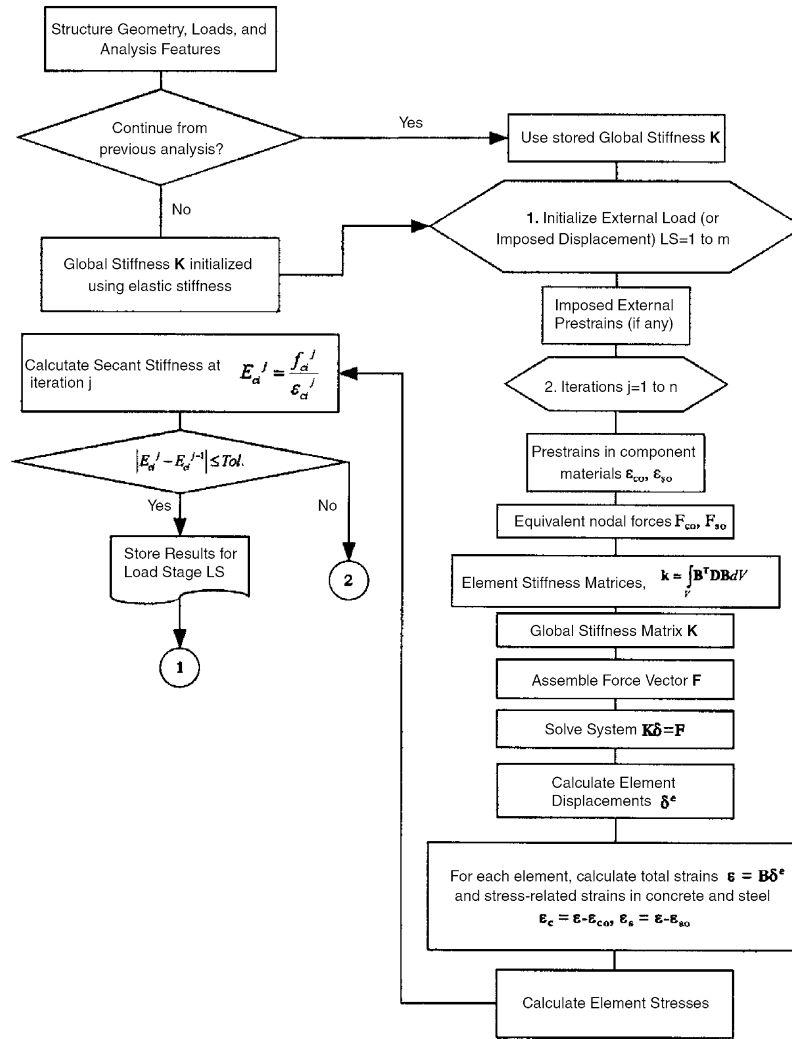
Fig. 2.   Flow chart of programs VecTor3 and VecTor6.

in the FRP at ultimate, which is low when compared to the given rupture strain. This was explained by the researchers as due to the nonuniform strain distribution at ultimate and large local strains in the FRP.

Table 2
Column properties, Demers and Neale columns

Carbon CFRP[a]	Thickness (layer) (mm)	E_j (MPa)	ε_{ju}					
	0.3	84,000	0.015					
Steel[b]	f_y (MPa)	E_s (MPa)						
	400	200,000						
Column	f_c' (MPa)	E_c^c (MPa)	ε_{co}	d_b (mm)	d_t (mm)	s (mm)	Corrosion simulated	Damage loading
U25-1	25	30600	0.0018	11.3	6.4	300	Yes	No
U25-2	25	22300	0.0021	16	11.3	150	No	No
U25-3	25	33800	0.0020	19.5	6.4	150	Yes	No
U25-4	25	25800	0.0021	25.2	11.3	300	No	No

[a] Manufacturer's properties for the fabric (carbon fibre plus epoxy binder).
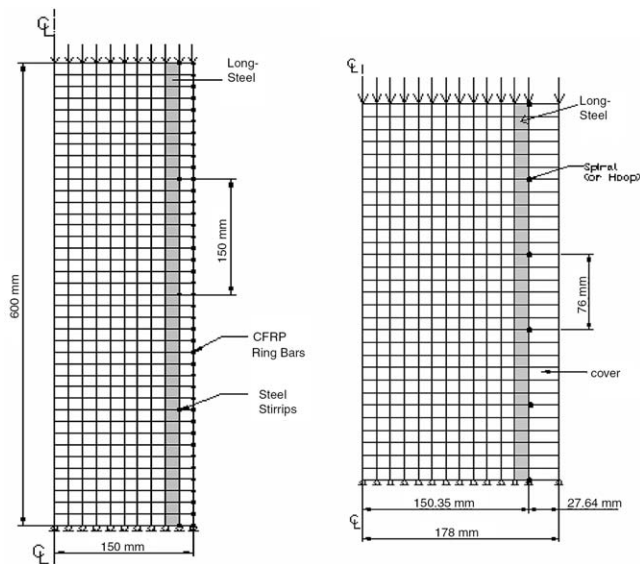[b] Assumed.
[c] From initial load of unconfined columns.

Fig. 3. Mesh details for Demers and Neale column U25-2 (left) and Toklucu column D14-H10M-P3.0 (right).

Fig. 4. Axial stress–axial strain curve, columns U25-2 and U25-4, Demers and Neale.

5.2. Toklucu columns [16]

The effects of confinement on concrete columns were further examined in a series of tests of circular columns subjected to axial compression. The concrete cylinder strength was 35 MPa. All columns had five bars of longitudinal steel. The properties for sample columns analyzed with VecTor6 are given in Table 4, where D is the diameter of the circular section, and ρ_l and ρ_v are the longitudinal and volumetric (transverse) steel ratio, respectively. f_y, f_u, ε_y are the yield strength, the ultimate strength, and strain at yield of the respective steels. The values for the concrete stiffness E_c and the strain at peak unconfined strength ε_{co} were assumed using the following formulae, which yield reasonable results for normal strength concrete:

$$E_c = 5000\sqrt{f_c'} \quad \varepsilon_{co} = \frac{2f_c'}{E_c} \tag{30}$$

The analytical model for a typical column (D14-H10M-P3.0) is shown in Fig. 3 (right). The model for concrete dilatation has no upper boundary for the maximum Poisson's ratio and therefore no limit to the possible lateral strains that the analytical column may reach. Due to the fact that concrete cover elements of these columns were not bounded by FRP composites, as was the case of the FRP-wrapped columns, and the four-node torus behaviour is limited to small deformations (not full Lagrangian elements), the cover elements were automatically deactivated in VecTor6 once their lateral stiffness decreased to a very small value (1% of the initial stiffness). This allowed for the continuation of imposed axial displacements after cover spalling until failure of the concrete core in the post-peak range. The axial load–axial strain curves for two columns and the axial load–spiral strain curve for one column are presented in Fig. 5 along with the analytical curves obtained with VecTor6 (solid thick lines). Comparison of the analytical and experimental results is given in Table 5.
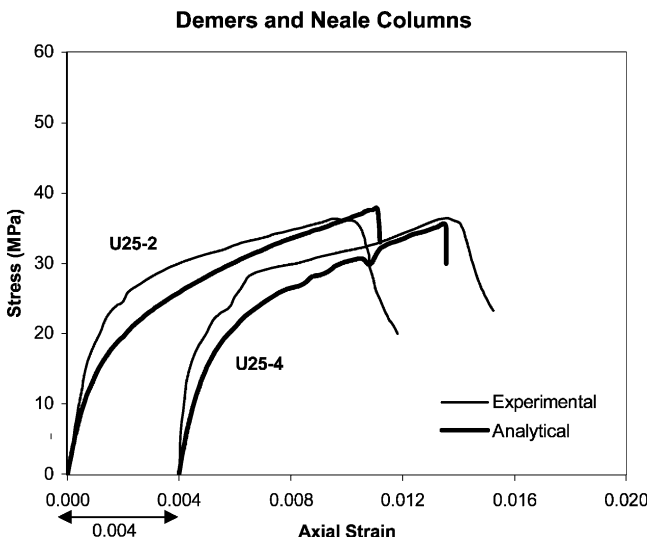
From the results, the experimental maximum load was well captured by the model. The average analyti-

Table 3
Analytical and experimental results, Demers and Neale columns

Column		Strength		P_{uc} (kN)	ε_{cc} (10^{-3})		ε_{cfu} (10^{-3})		ε_{fu} (10^{-3})
		(MPa)	Anal.\Exp.			Anal./Exp.		Anal./Exp.	
U25-1	Exp.	32.2	0.97	2460	3.80	1.76	4.90	1.37	3.70
	Anal.	31.2		2390	6.70		6.70		
U25-2	Exp.	36.6	1.03	2950	9.90	1.12	10.40	1.11	5.70
	Anal.	37.7		3030	11.10		11.10		
U25-3	Exp.	35.8	0.97	3080	6.60	1.41	6.90	1.35	4.30
	Anal.	34.7		3000	9.30		9.30		
U25-4	Exp.	37.0	0.96	3520	9.80	0.98	9.80	0.98	5.70
	Anal.	35.4		3410	9.60		9.60		

Table 4
Column properties, Toklucu

Column	Section			Longitudinal steel							Transverse steel						Concrete		
	D (mm)	Cover (mm)	d_b (mm)	Number bars	ρ_l (%)	f_y (MPa)	E_s (MPa)	ε_y (10^{-3})	f_u (MPa)	ε_{sh} (10^{-3})	d_t (mm)	ρ_v (%)	s (mm)	f_y (MPa)	ε_y (10^{-3})	f_u (MPa)	f'_c	E_c [a] (MPa)	ε_{co} [a] (10^{-3})
D14-S10M-P4.4	356	22	25.2	5	2.5	509	198,000	2.57	687	12.7	11.3	1.15	112	452	2.26	585	35.9	29,958	2.40
D14-H10M-P3.0	356	22	25.2	5	2.5	509	198,000	2.57	687	12.7	11.3	1.69	76	452	2.26	585	35.9	29,958	2.40
D10-S8M-P4.3	254	17	19.5	5	3.0	478	210,000	2.28	667	12.4	8.0	0.84	109	607	3.04	682	35.5	29,791	2.38
D10-SD4-P1.6	254	17	19.5	5	3.0	478	210,000	2.28	667	12.4	5.7	1.14	41	593	2.97	643	35.5	29,791	2.38
D8-SD5-P3.4	203	13	16.0	5	3.1	484	209,000	2.32	646	14.7	6.4	0.86	86	629	3.15	681	34.9	29,538	2.36
D8-SD5-P1.7	203	13	16.0	5	3.1	484	209,000	2.32	646	14.7	6.4	1.68	43	629	3.15	681	34.9	29,538	2.36
D8-S3/16-P1.7	203	13	16.0	5	3.1	484	209,000	2.32	646	14.7	4.7	0.93	43	620	3.10	689	34.9	29,538	2.36

[a] Calculated.
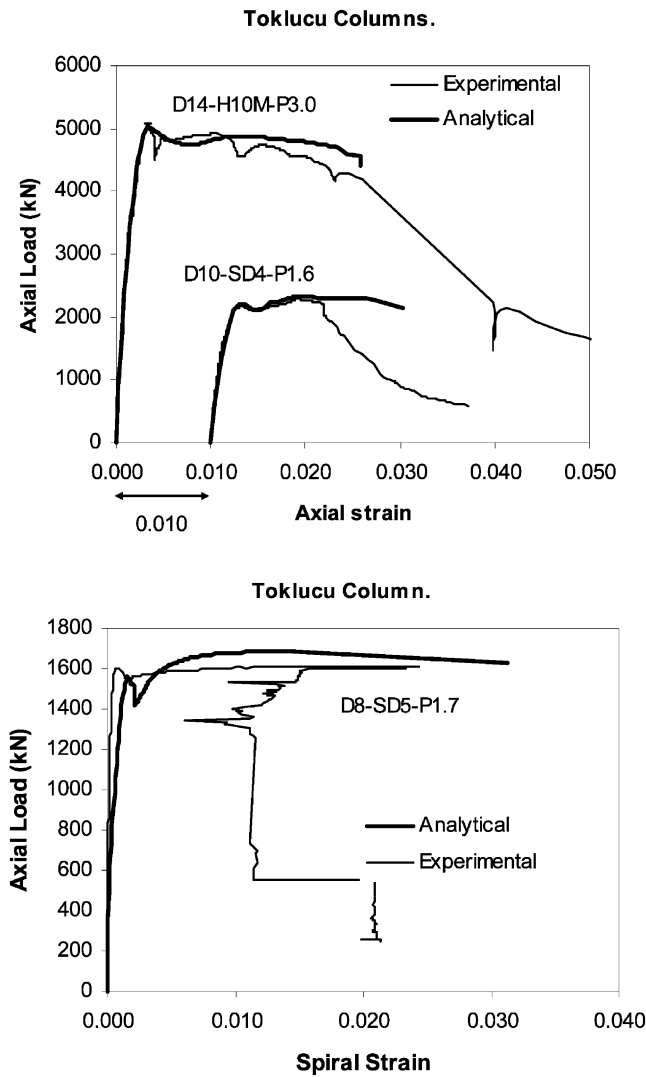
ties of the compression field modelling to reproduce the load capacity of these set of columns. The first and second peak strains are also well captured; after cover spalling, the analytical models showed some gain in strength and reached a second peak. The analytical pre-peak curves followed the initial loading path of the columns very closely, and the post-peak regime was reasonably traced. The onset of cover spalling in the models was at an axial strain between 2.30×10^{-3} and 2.50×10^{-3}, which was approximately the value for the peak unconfined concrete strain of the specimens, and compared well with the observed results. The spiral stress at the maximum concrete load was well captured in the case of well-confined columns. However, the lateral steel stress was overestimated for less well-confined columns indicating a lateral expansion larger than that observed.

5.3. Sheikh and Uzumeri columns [17]

The proposed models are also used to simulate the behaviour of rectangular columns subjected to axial compression. The columns analyzed are described in Table 6; concrete strength was between 35 and 40 MPa, tie spacing varied between $0.08b$ and $0.33b$, where b is the size of the column, and the number of longitudinal bars was 12 or 16. Table 6 shows the column properties following the same notation as that of the previous columns. The columns were square (i.e. $b = h$), and were 1960 mm in height. The finite element models for the columns consisted of eight-node concrete solids and truss bars. The longitudinal steel was smeared into the concrete solids and the tie steel was modelled using truss bars; the bar nodes were attached to the solid elements (perfect bond). One quarter of the cross-section of each column was modelled due to the symmetry of the load and the section. Sketches of the finite element meshes for each arrangement are shown in Fig. 6 and the tie and longitudinal arrangements for two of the columns analyzed are shown in the inset of

Fig. 5. Axial load–axial strain curve, Toklucu columns D10-H10M-P3.0, D10-SD4-P1.6 (left), axial load–spiral strain column D8-SD5-P1.7 (right).

cal-to-experimental P_{max} ratio was 1.01 with a coefficient of variation of 2.2%, demonstrating the capabili-

Table 5
Analytical and experimental results, Toklucu columns

Column	P_{max}			Peak axial strain (10^{-3})				Axial strain at spalling (10^{-3})		Spiral (hoop) stress at P_{cmax} (MPa)	
	Exp. (kN)	Anal. (kN)	Anal./Exp.	Exp.		Anal.		Exp.	Anal.	Exp.	Anal.
				1st	2nd	1st	2nd				
D14-S10M-P4.4	4350	4370	1.00	3.50	–	3.00	12.70	2.00	2.30	452	452
D14-H10M-P3.0	5100	5020	0.98	3.60	12.20	3.50	14.90	2.00	2.30	415	452
D10-S8M-P4.3	2270	2280	1.00	2.30	–	2.60	9.90	2.00	2.50	73	264
D10-SD4-P1.6	2290	2320	1.01	3.20	8.80	2.90	9.20	2.00	2.30	575	593
D8-SD5-P3.4	1460	1480	1.01	2.00	–	2.80	–	2.00	2.30	101	226
D8-SD5-P1.7	1610	1680	1.04	2.30	12.20	3.10	16.70	2.00	2.30	650	630
D8-S3/16-P1.7	1540	1500	0.97	3.50	–	3.00	9.70	2.00	2.50	400	620

Table 6
Column properties, Sheikh and Uzumeri

| Column	Section			Longitudinal steel									Transverse steel							Concrete		
	b (mm)	h (mm)	Cover (mm)	d_b (mm)	Number bars	ρ_l (%)	f_y (MPa)	E_s (MPa)	ε_y (10^{-3})	f_u (MPa)	E_{sh} (MPa)	ε_{sh} (10^{-3})	d_t (mm)	ρ_v (%)	s (mm)	f_y (MPa)	ε_y (10^{-3})	f_u (MPa)	ε_{sh} (10^{-3})	f'_c (MPa)	E_c (MPa)	ε_{co} (10^{-3})
4C4-12	305	305	17	15.9	16	3.44	407	206,700	1.97	6.35	8268	7.20	3.2	1.52	25.4	634	3.17	760	–	40.8	31,933	2.20
4B3-19	305	305	15	19.1	12	3.67	391	196,365	1.99	540	6235	7.80	7.9	1.80	101.6	480	2.40	500	–	33.4	28,904	2.20
4B4-20	305	305	17	19.1	12	3.67	391	196,365	1.99	540	6235	7.80	4.8	1.70	38.1	480	2.40	540	–	34.7	29,435	2.20
4D3-22	305	305	15	19.1	12	3.67	391	196,365	1.99	540	6235	7.80	7.9	1.60	82.6	480	2.40	500	–	35.5	29,784	2.20
4D6-24	305	305	16	19.1	12	3.67	391	196,365	1.99	540	6235	7.80	6.4	2.30	38.1	480	2.40	510	–	35.8	29,928	2.20
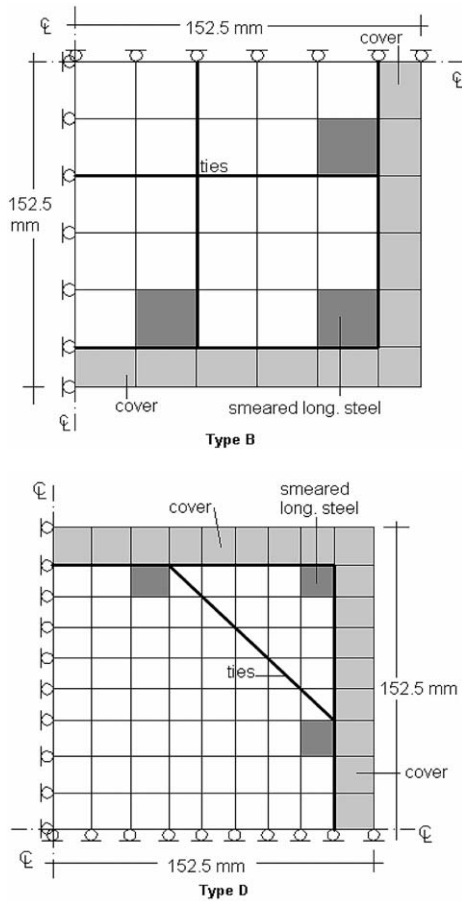
Fig. 6.   Mesh details for Sheikh and Uzumeri columns.

Fig. 7. Cover elements were automatically deactivated in VecTor3 once their lateral stiffness decreased to 1% of the initial stiffness. The axial load–strain curves for
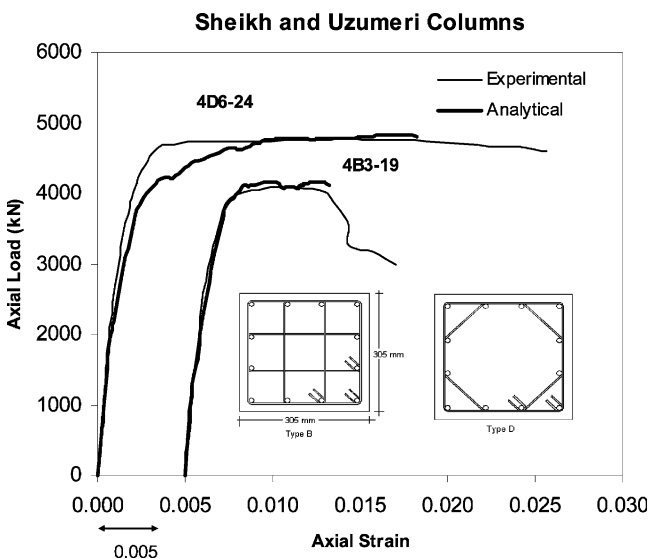

Fig. 7.   Sheikh and Uzumeri columns 4D6-24, 4B3-19.

two of the columns are presented in Fig. 7, along with the analytical curves obtained with VecTor3 (solid thick lines).

Analytical and experimental results are shown in Table 7. Concrete cover begins to spall at axial strains close to the recorded experimental values. Also, the overall average strain in the tie steel at the maximum concrete load reasonably compares with those obtained from the experiments. The pre- and post-peak responses were captured well, and the maximum analytical to experimental load ratio reached an average of 1.02 with a coefficient of variation of 1.0%.

6. Comments and limitations

The nonlinear analytical solution was obtained using controlled displacements and the secant stiffness matrices of the finite elements were updated during each iteration of every load stage until convergence was attained. This method provides a stable solution as the secant stiffness is always positive. Load-increment solution methods such the arc-length method were not implemented in the solution strategy.

The analytical stress–strain curve obtained from a confined structural element subjected to monotonic axial compression can be used to analyze a similar reinforced concrete section when subjected to cyclic loading or flexural bending. A linear segmental approach can easily be implemented for the calculation of its moment–curvature diagram (see [9]).

Overestimation of concrete expansion may occur when using the proposed model (Eq. (1)). However, a trend between the confinement level and the concrete strength was found when developing this equation. Also, in the analytical models for the columns, size effect was not investigated and may have an influence in the response of slender columns subjected to axial compression. The effect of buckling of bars on the reinforced column response was not considered in the analytical solutions.

Finally, the termination of the numerical analysis at post-peak stages earlier than the experimental curves observed in some cases, was likely the result of overestimation of the dilatation and the use of small-deformation finite elements. Full Lagrangian elements can be used to model the large lateral deformations that confined concrete may experience, as well as second-order effects (i.e. geometrical stability).

7. Conclusion

Newly developed confinement models were implemented in the nonlinear finite element programs VecTor6 and VecTor3 to analyze reinforced concrete columns confined with steel and/or FRP wraps. The

Table 7
Analytical and experimental results, Sheikh and Uzumeri

Column	P_{max}			Peak axial strain (10^{-3})				Axial strain at spalling (10^{-3})		Tie stress at P_{cmax} (MPa)	
	Exp. (kN)	Anal. (kN)	Anal./Exp.	Exp.		Anal.		Exp.	Anal.	Exp.	Anal.
				1st	2nd	1st	2nd				
4C4-12	4915	5094	1.04	5.20	20.50	7.00	–	1.5–2.0	2.10	469	582
4C3-19	4092	4168	1.02	6.10	–	7.50	–	1.5–2.0	1.40	400	300
4B4-20	4368	4416	1.01	8.00	–	5.10	12.00	1.5–2.0	1.80	544	494
4D3-22	4301	4438	1.03	4.10	–	6.50	–	1.5–2.0	1.50	386	385
4D6-24	4723	4831	1.02	3.70	17.70	3.90	16.80	1.5–2.0	1.70	475	480

objective was to evaluate the capabilities of the compression field modelling to reproduce the behaviour of confined concrete at the structural level. The analytical and experimental results were found to agree reasonably well. The proposed stress–strain formulation and strength enhancement model represent an improved comprehensive approach to the modelling of confined concrete, compatible with nonlinear finite element analysis techniques.

Acknowledgements

References

[1] Collins MP, Mitchel D. Prestressed concrete structures, 1st ed.. Toronto and Montreal, Canada: Response Publications; 1997.

[2] Vecchio FJ, Collins MP. The modified compression field theory for reinforced concrete solids subjected to shear. J Am Conc Inst 1986;83(2):219–31.

[3] Selby RG, Vecchio FJ. A constitutive model for analysis of reinforced concrete solids. Can J Civ Eng 1997;24:460–70.

[4] Selby RG, Vecchio FJ. Three-dimensional analysis of reinforced concrete solids. Civil Engineering Report, University of Toronto, Toronto, Canada; 1993.

[5] Montoya E, Vecchio FJ, Sheikh SA. Compression field modeling of confined concrete. Struct Eng Mech 2001;12(3):231–48.

[6] Karabinis AI, Rousakis TC. Concrete confined by FRP material: a plasticity approach. Eng Struct 2002;24:923–32.

[7] Pivonka P, Lackner R, Mang H. Numerical analyses of concrete subjected to triaxial compressive loading. European Congress on Computation Methods in Applied Mechanics, ECCOMAS 2000, Barcelona. 2000, p. 26.

[8] Ghazi M, Attard MM, Foster SJ. Modelling triaxial compression using the Microplane formulation for low confinement. Comp Struct 2002;80:919–34.

[9] Montoya E. Behavior and analysis of confined concrete. PhD Thesis, Department of Civil Engineering, University of Toronto, Toronto, Canada; 2003.

[10] Imran I, Pantazopoulou SJ. Experimental study of plain concrete under triaxial stress. ACI Mat J 1996;93(6):589–601.

[11] Hoshikuma J, Kazuhiko K, Kazuhiko N, Taylor AW. A model for confinement effect on stress–strain relation of reinforced concrete columns for seismic design. Proceedings of the 11th World Conference on Earthquake Engineering. London, UK: Elsevier Science; 1996, p. 825.

[12] Yamamoto T, Vecchio FJ. Analysis of reinforced concrete shells for transverse shear and torsion. ACI Struct J 2001;98(2): 191–200.

[13] Vecchio FJ. Finite element modeling of concrete expansion and confinement. J Struct Eng ASCE 1992;118(9):2390–406.

[14] Kupfer H, Hilsdorf HK, Rusch H. Behavior of concrete under biaxial stresses. ACI J 1969;66–52:656–66.

[15] Demers M, Neale KW. Confinement of reinforced concrete columns with fibre-reinforced composite sheets—an experimental study. Can J Civ Eng 1999;26:226–41.

[16] Toklucu MT. Behavior of reinforced concrete columns confined with circular spiral and hoops. MASc Thesis, University of Toronto, Toronto, Canada; 1992.

[17] Sheikh SA, Uzumeri SM. Strength and ductility of tied concrete columns. J Struct Div 1980;106(sT5):1079–112.